

From Continuous sEMG Signals to Discrete Muscle State Tokens: A Robust and Interpretable Representation Framework

Yuepeng Chen^{a,b,1}, Kaili Zheng^{c,1}, Ji Wu^{c,d,e,*}, Zhuangzhuang Li^c, Ye Ma^f, Dongwei Liu^g, Chenyi Guo^{c,d,*} and Xiangling Fu^{a,b,*}

^aSchool of Computer Science (National Pilot Software Engineering School), Beijing University of Posts and Telecommunications, Beijing, China

^bKey Laboratory of Trustworthy Distributed Computing and Service (BUPT), Ministry of Education, Beijing, China

^cDepartment of Electronic Engineering, Tsinghua University, Beijing, China

^dInstitute for Precision Medicine, Tsinghua University, Beijing, China

^eCollege of AI, Tsinghua University, Beijing, China

^fResearch Academy of Grand Health, Ningbo University, Ningbo, China

^gSchool of Information Technology and Artificial Intelligence, Zhejiang University of Finance and Economics, Hangzhou, China

ARTICLE INFO

Keywords:

Surface electromyography
Tokenization
Muscle activation representation
Action recognition
Movement quality assessment

ABSTRACT

Surface electromyography (sEMG) signals exhibit substantial inter-subject variability and are highly susceptible to noise, posing challenges for robust and interpretable decoding. To address these limitations, we propose a discrete representation of sEMG signals based on a physiology-informed tokenization framework. The method employs a sliding window aligned with the minimal muscle contraction cycle to isolate individual muscle activation events. From each window, ten time–frequency features, including root mean square (RMS) and median frequency (MDF), are extracted, and K-means clustering is applied to group segments into representative muscle-state tokens. We also introduce a large-scale benchmark dataset, ActionEMG-43, comprising 43 diverse actions and sEMG recordings from 16 major muscle groups across the body. Based on this dataset, we conduct extensive evaluations to assess the inter-subject consistency, representation capacity, and interpretability of the proposed sEMG tokens. Our results show that the token representation exhibits high inter-subject consistency (Cohen’s Kappa = 0.82 ± 0.09), indicating that the learned tokens capture consistent and subject-independent muscle activation patterns. In action recognition tasks, models using sEMG tokens achieve Top-1 accuracies of 75.5% with ViT and 67.9% with SVM, outperforming raw-signal baselines (72.8% and 64.4%, respectively), despite a 96% reduction in input dimensionality. In movement quality assessment, the tokens intuitively reveal patterns of muscle underactivation and compensatory activation, offering interpretable insights into neuromuscular control. Together, these findings highlight the effectiveness of tokenized sEMG representations as a compact, generalizable, and physiologically meaningful feature space for applications in rehabilitation, human–machine interaction, and motor function analysis.

1. Introduction

Human movement is controlled by the nervous system, which generates and transmits signals to motor units, leading to the activation and contraction of muscle fibers (Heckman and Enoka, 2012; Milner-Brown et al., 1973). Surface electromyography (sEMG) captures the electrical activity generated by these muscle fibers through non-invasive electrodes placed on the skin. These signals represent the summation of motor unit action potentials (Day and Hulliger, 2001). The amplitude and frequency characteristics of sEMG signals correlate with muscle activation intensity and timing, offering insights into muscle force (Disselhorst-Klug et al., 2009; Staudenmann et al., 2010), fatigue (Cifrek et al., 2009), and coordination (Tu et al., 2023). Consequently, sEMG has been widely utilized in biomechanics (Bonato et al., 2002; Valentin and Zsoldos, 2016; Taborri et al., 2020), rehabilitation (Disselhorst-Klug and Williams, 2020; Khoshdel et al., 2018; Delph et al., 2013), and motion analysis (Frigo and Crenna, 2009; Kotov-Smolenskiy et al., 2021; Kim et al., 2018).

*Corresponding author

✉ wuji_ee@tsinghua.edu.cn (J. Wu); guochy@mail.tsinghua.edu.cn (C. Guo); fuxiangling@bupt.edu.cn (X. Fu)

ORCID(s): 0000-0001-6170-726X (J. Wu); 0000-0002-8222-5179 (C. Guo); 0000-0002-1492-2829 (X. Fu)

¹These authors contributed equally to this work.

The analysis of sEMG signals typically begins with a series of preprocessing steps, including filtering, rectification, and envelope extraction, to facilitate the quantitative assessment of neuromuscular activity (Boudreau et al., 2009; Torres-Peralta et al., 2014; Lacerda et al., 2019; Özgünen et al., 2010), such as muscle activation evaluation. Based on the preprocessed signals, handcrafted features are often extracted from the time, frequency, or time-frequency domains, and then fed into traditional machine learning classifiers such as Linear Discriminant Analysis (LDA) (Zhang et al., 2013; PRASAD et al., 2024), k-Nearest Neighbor (KNN) (Bezrukov et al., 2024), or Support Vector Machine (SVM) (She et al., 2010; Nazmi et al., 2024), for pattern recognition tasks. In recent years, deep learning models have been increasingly introduced to automate feature extraction and improve classification performance (Sun et al., 2024a; Wei et al., 2019). Among them, spectrogram-based methods have become particularly prominent: raw sEMG signals are transformed into two-dimensional time-frequency representations (e.g., spectrograms), which are then processed by convolutional neural networks to extract discriminative spatial features (Barona López et al., 2024). Moreover, Transformer architectures have been explored to model temporal dependencies in sEMG signals (Montazerin et al., 2022; Wang et al., 2024), aiming to capture the dynamic characteristics of muscle activation more effectively.

Despite the substantial progress, existing approaches still face several significant challenges. A key challenge in processing and decoding sEMG signals to extract critical information about muscle control lies in their complexity. On one hand, sEMG signals are susceptible to various noise sources, such as suboptimal electrode-skin contact and electrical interference. These factors can significantly degrade signal quality and complicate the accurate extraction of meaningful data. Although noise reduction methods such as EWT-IIT (Xiao, 2022), Singular Value Decomposition (SVD) (Zhang et al., 2012), and Modified Spectral Subtraction (Cvetković et al., 2024) have been proposed, they are hindered by challenges such as complex threshold selection, high computational costs, or a trade-off in accuracy. On the other hand, sEMG data are highly subject-dependent, influenced by individual differences in skin thickness, subcutaneous fat, and electrode placement. Additionally, the psychological state, including emotional state and attention levels, may also contribute to this inter-subject variability (Ait Yous et al., 2025). These variations further complicate the interpretation of sEMG signals, making it difficult to establish universal models for muscle control. To address this challenge, transfer learning models and normalization techniques have been proposed, but they still face specific limitations. Transfer learning models (Lin et al., 2024) require extensive subject-specific data for fine-tuning, while normalization techniques, such as Maximal Volitional Contraction (MVC)-based normalization (Martens et al., 2015), can be unreliable due to variations in an individual's ability to perform maximal contractions.

We argue that the fundamental limitation in sEMG modeling lies in its reliance on continuous, high-resolution time-series signals, which are often redundant and susceptible to local perturbations. For many downstream applications such as action recognition and movement quality assessment, maintaining exact signal fidelity at the raw level is not strictly necessary. Instead, capturing the essential patterns of muscle activation in a compact, structured representation can enhance robustness, computational efficiency, and interpretability. Recent advances in representation learning for non-text modalities have demonstrated the effectiveness of such compact, symbolic representations through tokenization. In speech and audio modeling, methods such as AudioLM (Borsos et al., 2023), HuBERT (Hsu et al., 2021), SoundStream (Zeghidour et al., 2021) and EnCodec (Défossez et al., 2022) convert raw waveforms into discrete or low-dimensional token sequences that capture essential acoustic or phonetic structures. These tokenized representations have been shown to improve generalization, reduce computational burden, and facilitate cross-modal alignment with other data types such as text or video. Given the shared temporal dynamics, hierarchical structure, and signal variability between speech and physiological signals, such tokenization strategies hold strong potential for sEMG modeling.

However, tokenization has not yet been systematically explored for sEMG signals. Unlike image or audio data, sEMG reflects physiologically structured muscle activation patterns that are not directly observable but are temporally and functionally organized. This necessitates a new form of tokenization—one grounded not in visual or phonetic primitives, but in the functional states of muscle contraction. To this end, we propose a physiology-driven tokenization framework for sEMG, which discretizes raw signals into interpretable and reusable symbols aligned with muscle contraction states. The process begins with the extraction of informative time- and frequency-domain features, such as root mean square (RMS) and zero-crossing (ZC), from sliding signal segments. These segments are then clustered using the K-means algorithm to identify a finite set of prototypical muscle activation patterns. An overview of the method is illustrated in Fig. 1. The resulting patterns serve as reusable sEMG tokens, abstracting away low-level noise while preserving essential motor information.

To support the development and evaluation of our method, we present ActionEMG-43, a large-scale dataset containing 43 actions recorded from 14 subjects muscle coverage spanning the upper and lower body. The dataset

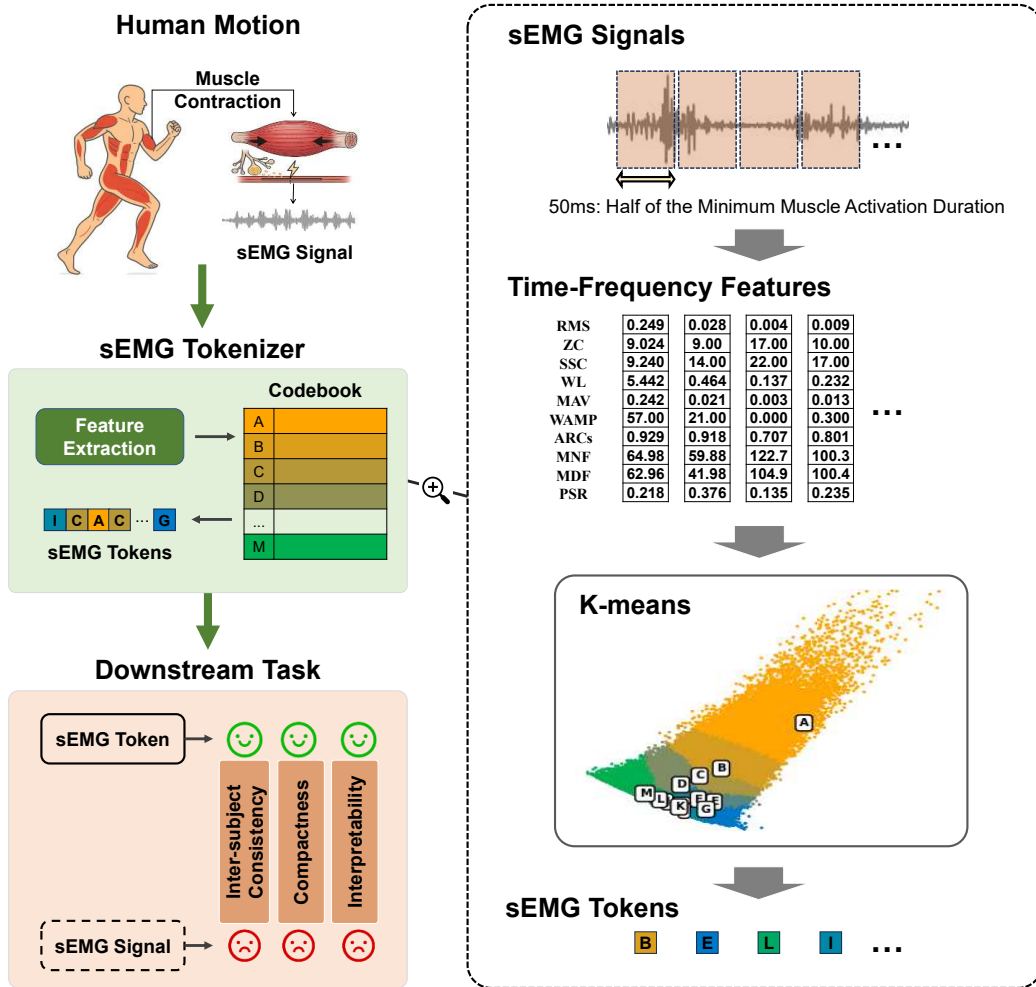


Figure 1: Overview of the sEMG tokenization process. sEMG signals are segmented using a sliding window, and features of all segments are clustered via K-means to generate a codebook of representative muscle activation states. New sEMG data are mapped to discrete tokens by assigning each segment to the nearest cluster centroid in the pre-established codebook, resulting in a symbolic representation that enhances inter-subject consistency, compactness and interpretability for downstream tasks.

provides high-resolution, multi-channel sEMG signals along with action annotations, and serves as a comprehensive benchmark for evaluating tokenization methods, action recognition, and movement quality assessment.

Based on this dataset, we evaluate the inter-subject consistency, representation capacity, and interpretability of the proposed sEMG tokens representations. In the inter-subject consistency analysis, sEMG tokens exhibit strong agreement across individuals, achieving an average overlap rate of 83.78% and a Cohen's Kappa of 0.82, highlighting their robustness and generalizability. In the action recognition experiment, both SVM and Vision Transformer (ViT) models using sEMG tokens as input outperform those using raw signals, with over 3% improvements in Top-1 accuracy and F1 score. Notably, this performance gain is achieved alongside a reduction of over 96% in input dimensionality, significantly improving computational efficiency without sacrificing accuracy. Furthermore, movement quality assessment experiments show that sEMG tokens effectively distinguish between expert and novice participants, revealing key neuromuscular differences such as muscle underactivation and compensatory activation. These results demonstrate the potential of token-based representations for interpretable and personalized rehabilitation assessment and feedback. These experiments demonstrate that the proposed sEMG tokens representation effectively mitigates key

limitations of raw sEMG signals—including susceptibility to noise and high subject dependency—while offering a compact, generalizable, and interpretable feature space for downstream motor analysis tasks.

To summarize, the main contributions of this study are as follows:

- We introduce the first physiology-informed tokenization framework for sEMG, which maps raw signals into discrete and interpretable symbols aligned with functional muscle contraction states.
- We present ActionEMG-43, a large-scale sEMG dataset comprising 43 diverse actions collected from 16 muscle groups across the upper and lower limbs. The dataset offers fine-grained recordings to support research on muscle activation modeling and downstream motor tasks.
- We empirically demonstrate that the proposed sEMG tokens exhibit strong inter-subject consistency, retain essential discriminative information for action recognition, and enable interpretable assessment of motor performance, including detection of underactivation and compensatory patterns.

2. Related Work

2.1. Continuous sEMG Signals Analysis

sEMG is a continuous-valued amplitude signal that reflects dynamic neuromuscular activation. With the advancement of deep learning, data-driven architectures such as convolutional neural networks (CNNs) and Transformers have been widely applied to sEMG analysis (Bittibssi et al., 2021; Montazerin et al., 2022; Gan et al., 2025). These approaches typically take raw waveforms or time–frequency spectrograms as input and learn discriminative features through end-to-end training, achieving substantial performance improvements in downstream tasks such as classification and regression. However, sEMG signals are highly sensitive to electrode placement, skin impedance, and inter-subject physiological differences, which often leads to performance degradation across subjects or experimental conditions (Zhang et al., 2025). To address this issue, prior studies have explored strategies at both the data and model levels. At the data level, some works employ generative adversarial networks (GANs) to synthesize perturbed signal samples, thereby improving robustness to noise and variations in recording conditions (Lin et al., 2023; Nasrallah et al., 2023; Li et al., 2026). At the model level, transfer learning and cross-subject training schemes have been introduced to mitigate performance drops caused by inter-individual variability (Côté-Allard et al., 2017; Fan et al., 2023; Fratti et al., 2024). Despite these efforts, the observed improvements in generalization largely rely on data scale and training mechanisms rather than structural constraints at the representation level. Moreover, continuous amplitude representations lack explicit structural semantics, making it difficult to characterize inter-muscle coordination patterns and their interpretable relationships.

2.2. Discrete Muscle Activation Detection

To enhance interpretability, several studies have explored discrete representations of muscle activation. A common strategy is to partition sEMG signals into activation and non-activation phases using threshold-based detection or onset–offset analysis (Micera et al., 1998; Morantes et al., 2013; Kang et al., 2020; G B et al., 2023; Huang et al., 2025). This binary state modeling approach has been widely applied in gait analysis and rehabilitation assessment. Although such methods improve interpretability, they are typically limited to coarse binary segmentation and fail to capture fine-grained variations in contraction intensity. Furthermore, most prior work has focused on single-muscle analysis or limited multi-channel settings, without explicitly modeling the structured temporal interactions among multiple muscles.

3. Material and methods

3.1. ActionEMG-43 Dataset

To support research in sEMG-based motion analysis, we present ActionEMG-43, a large-scale dataset designed to benchmark a wide range of tasks including action recognition, tokenization-based representation learning, and movement quality assessment.

As presented in Table 1, ActionEMG-43 is the most comprehensive and versatile sEMG dataset to date. It comprises 43 distinct actions, encompassing a broad spectrum of daily and exercise-related movements such as jogging, high knee lifts, frog jumps, high kicks, and squats. A full list of the actions is provided in Appendix Table. 5. The data

Table 1

Comparison of publicly available sEMG datasets in terms of subject count, anatomical coverage, number of muscle groups, and action diversity. ActionEMG-43 offers the most comprehensive coverage, spanning the whole body with 16 muscle groups and 43 distinct actions, providing a benchmark for large-scale motor analysis.

Name	Year	# Subjects	Body Region	# Muscle Groups	# Actions
EMAHA-DB1 (Karnam et al., 2023)	2023	24	right arm	5	22
MyoBit (Chen et al., 2023)	2023	7	elbow	1	7
SIAT-LLMD (Wei et al., 2023)	2023	40	left leg	9	16
JJ dataset (Sun et al., 2024b)	2024	15	left leg	9	10
ULTRA-MoCap (Fritsche et al., 2025)	2025	13	upper body	3	5
ActionEMG-43	2025	14	whole body	16	43

were collected from 14 healthy adult participants (aged 21–36 years, mean \pm std: 27.7 ± 5.1 years), with each subject performing at least three repetitions of each cyclical movement and maintaining each static or continuous movement for a minimum of two seconds. The sEMG signals were recorded using Delsys Trigno wireless sensors from 16 major muscle groups, providing extensive coverage of both upper and lower limbs as well as trunk muscles. Sensor placement is illustrated in Fig. 2. The signals were sampled at 1259 Hz, ensuring high temporal resolution for detailed time-frequency analysis.

To further validate the interpretability of sEMG tokens in real-world skill evaluation scenarios, we constructed a focused benchmark named the MovEMENT Quality Assessment Dataset (MEQAD). While ActionEMG-43 provides large-scale coverage for modeling diverse motor patterns, MEQAD complements it by targeting fine-grained differences in movement execution quality. It includes three representative actions—High Knees, Squats, and Biceps Curls—with both standard and commonly observed faulty versions. One subject, a Certified Strength and Conditioning Specialist (CSCS) accredited by the National Strength and Conditioning Association (NSCA), performed both correct and faulty executions as reference demonstrations. Two additional participants without professional training backgrounds imitated both versions under expert supervision. The data collection protocol mirrors that of ActionEMG-43, using identical sensor configurations, sampling rates, and muscle group coverage. Detailed descriptions of movement variations and instruction procedures are provided in Appendix A.

Based on the two datasets described above, we systematically evaluate the proposed tokenization framework across multiple dimensions. Using ActionEMG-43, we assess the inter-subject consistency and representation capacity of sEMG tokens in large-scale action recognition tasks. In addition, MEQAD enables fine-grained analysis of movement quality, allowing us to validate the interpretability of tokenized representations in capturing underactivation, compensatory patterns, and other execution-level differences. These evaluations demonstrate the effectiveness of our approach in both general motor decoding and personalized assessment scenarios.

In our experiments, we employ a five-fold cross-validation strategy unless otherwise specified. In each fold, samples from a subset of subjects are used for validation, and samples from the remaining subjects were used for training. Both the cluster centers and the downstream-task models are trained on the training set, and the experimental results reported in this paper are based on the validation set. This approach ensures that the training and validation subsets are completely separate, preventing any information leakage during both the tokenization and model training processes.

3.2. Tokenization

The raw sEMG signals are first bandpass filtered between 20 and 450 Hz to remove low-frequency noise and high-frequency disturbances, using a 4th-order Butterworth filter, following common practices in previous studies (Merletti and Farina, 2016; Moreira et al., 2021; Lim et al., 2024; Douglas et al., 2025). Subsequently, the long signals are divided into segments. One of the fundamental responses of muscle fibers to brief stimulation is a twitch. According to previous studies (Jenkins and Tortora, 2016; Carlson, 2018), a single twitch typically lasts around 100 milliseconds and consists of three phases: the latent period, contraction phase, and relaxation phase. Based on this, we segment sEMG signals using a sliding window of 50 ms with a stride of 25 ms, to efficiently capture the detailed variations within each muscle twitch for a more comprehensive understanding. Ten conventional time-domain and frequency-domain features are then extracted from each sEMG segment: Root Mean Square (RMS), Zero Crossing (ZC), Slope Sign Change (SSC), Waveform Length (WL), Mean Absolute Value (MAV), Wilson Amplitude (WAMP), Autoregressive Coefficients (ARCs), Mean Frequency (MNF), Median Frequency (MDF), and Power Spectrum Ratio (PSR). These

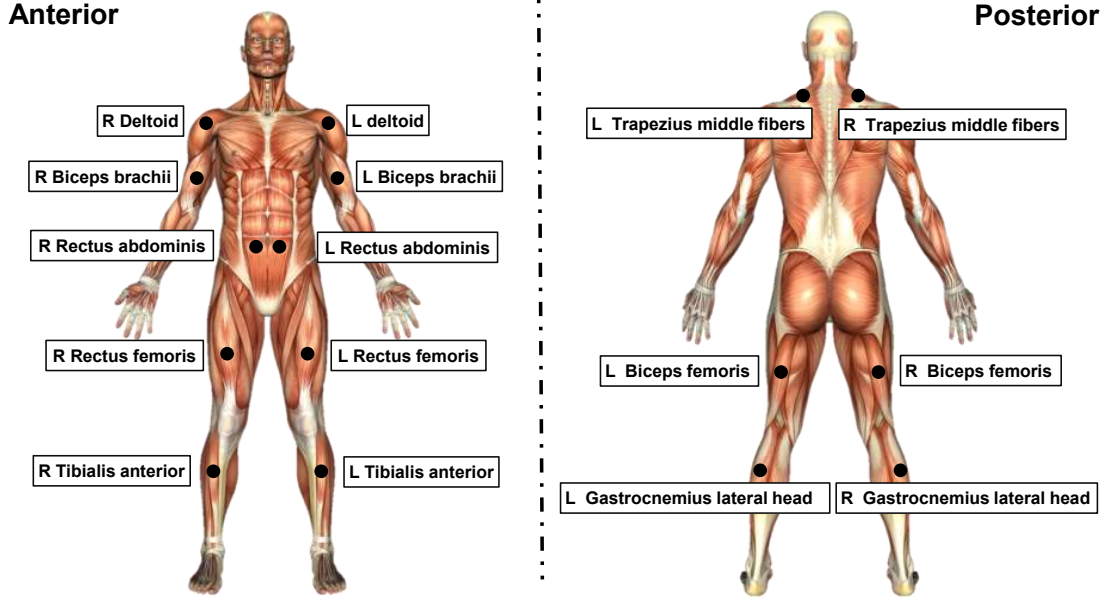


Figure 2: Muscle Groups for sEMG Signals Collection in ActionEMG-43. sEMG signals were recorded from 16 major muscle groups across the upper limbs, lower limbs, and trunk using Delsys Trigno wireless sensors. This comprehensive coverage enables detailed analysis of whole-body motor coordination and muscle activation patterns across a wide range of actions.

features are commonly used in previous studies (Duan et al., 2023; Atzori et al., 2014; Phinyomark et al., 2012). Denote the feature vectors of all segments as $\mathcal{F} = \{f_1, f_2, \dots, f_N\}$, $f_n \in \mathbb{R}^d$, where N is the total number of sEMG segments in the training set and d is the number of time-frequency features ($d = 10$ in this study).

During training, the K-means algorithm is applied to cluster the feature vectors by minimizing the within-cluster variance:

$$\arg \min_{\{C_k\}} \sum_{k=1}^K \sum_{f_n \in C_k} \|f_n - \mu_k\|^2 \quad (1)$$

where C_k denotes the set of feature vectors assigned to the k -th cluster and $\mu_k \in \mathbb{R}^d$ is the centroid (cluster center) of C_k . The optimized centroids $\{\mu_1, \mu_2, \dots, \mu_K\}$ constitute a data-driven codebook that captures representative muscle activation patterns. For clarity of notation, we denote each cluster and its corresponding discrete token by an uppercase letter from the set $\{A, B, \dots, Z\}$, assuming $K \leq 26$.

During inference, a new feature vector f_i extracted from an unseen sEMG segment is mapped to its nearest cluster center to obtain a symbolic token s_i :

$$s_i = \arg \min_k \|f_i - \mu_k\|^2 \quad (2)$$

In this way, continuous sEMG signals are transformed into a sequence of discrete tokens, providing a compact and symbolic representation of muscle activation over time.

3.3. Model Selection

To determine the optimal number of clusters for sEMG tokenization, we evaluate both intra-cluster compactness and clustering discriminability using two complementary metrics: Sum of Squared Errors (SSE) and Phone-normalized Mutual Information (PNMI).

1. Sum of Squared Errors (SSE)

$$\text{SSE} = \sum_{k=1}^K \sum_{x_i \in C_k} \|x_i - \mu_k\|^2 \quad (3)$$

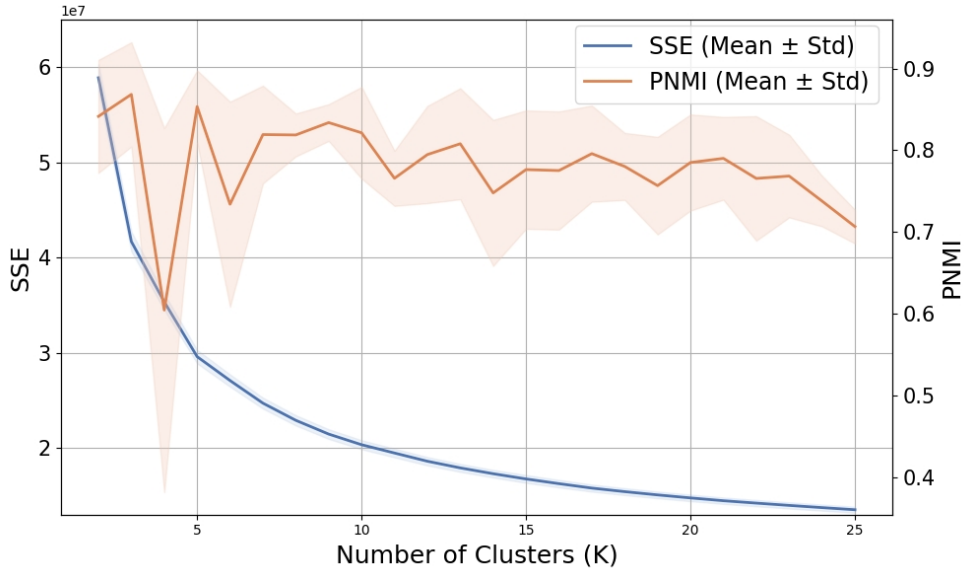


Figure 3: Trends of SSE and PNMI with respect to the number of clusters K (ranging from 2 to 25). Curve shows the average result over five-fold cross-validation, and the shaded area represents the standard deviation across folds.

Here, K denotes the number of clusters; C_k is the set of feature vectors assigned to the k -th cluster; and $\mu_k \in \mathbb{R}^d$ represents its centroid. SSE quantifies clustering compactness by aggregating the squared Euclidean distances between each feature vector and its assigned centroid. As K increases, SSE naturally decreases due to finer partitioning, but the marginal gain diminishes. A plateau in the SSE curve typically indicates the onset of diminishing returns, suggesting a suitable range for K .

2. Phone-normalized Mutual Information (PNMI)

To evaluate clustering discriminability, we use the Phone-normalized Mutual Information (PNMI) (Hsu et al., 2021), an information-theoretic metric originally proposed for unsupervised speech tokenization. Given a reference token sequence $[y_1, y_2, \dots, y_T]$ and a predicted token sequence $[t_1, t_2, \dots, t_T]$, the joint distribution is estimated as:

$$p_{y,t}(i, j) = \frac{1}{T} \sum_{t=1}^T [y_t = i \wedge t_t = j] \quad (4)$$

PNMI is then computed as:

$$\text{PNMI} = \frac{I(y; t)}{H(y)} = \frac{\sum_i \sum_j p_{y,t}(i, j) \log \frac{p_{y,t}(i, j)}{p_y(i)p_t(j)}}{\sum_i p_y(i) \log p_y(i)} = \frac{H(y) - H(y | t)}{H(y)} = 1 - \frac{H(y | t)}{H(y)} \quad (5)$$

where $I(y; t)$ is the mutual information and $H(y)$ is the entropy of the reference sequence. Higher PNMI indicates better agreement between the two sequences.

We systematically evaluate both SSE and PNMI for cluster numbers K ranging from 2 to 25. All experiments are conducted under a five-fold cross-validation protocol to ensure robustness. As shown in Figure 3, the SSE curve flattens noticeably around $K = 15$, indicating reduced benefit from increasing cluster numbers. Meanwhile, PNMI reaches a relative peak at $K = 13$, suggesting optimal alignment between the predicted and reference token structures. Based on this joint evaluation of compactness and consistency, we select $K = 13$ as the final number of clusters. Each cluster centroid is then assigned a unique symbolic label from the set $\{A, B, C, \dots, M\}$, forming the discrete sEMG tokens vocabulary used throughout subsequent analyses.

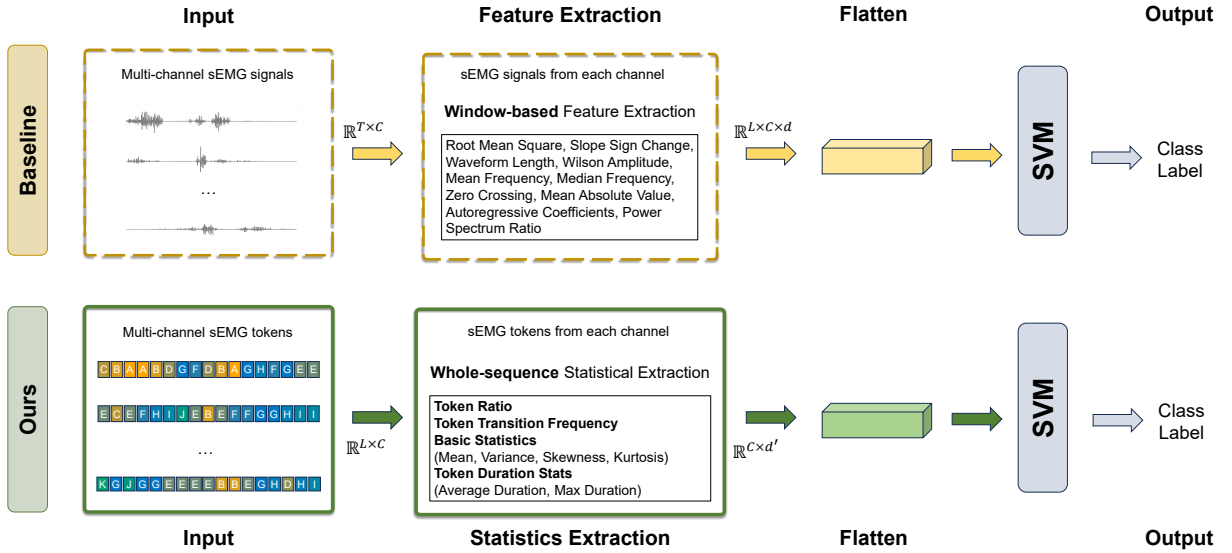


Figure 4: SVM-based human action recognition model. Time-frequency features from raw sEMG signals or statistical descriptors from sEMG tokens are flattened into one-dimensional vectors and used as input for classification.

3.4. Downstream Task Setup

Experiments on two downstream tasks, human action recognition and movement quality assessment, are conducted to demonstrate the representation capacity and interpretability of the proposed sEMG tokens representation respectively. This section details the model architectures used for action recognition and the methodology for quantifying execution quality in movement assessment.

3.4.1. Human Action Recognition Models

To evaluate the representational capacity of sEMG tokens, we compare their performance with raw sEMG signals on a human action recognition task using two representative classification models: Support Vector Machine (SVM) (Oskoei and Hu, 2008) as a baseline traditional machine learning method, and Vision Transformer (ViT) (Montazerin et al., 2022) as a state-of-the-art deep learning approach. The architecture of the SVM-based model is illustrated in Figure 4, while the ViT-based model is shown in Figure 5. As both models require fixed-length input, we standardize all input sequences to L segments via replication-padding, which corresponds to padding raw sEMG signals to T sampling points. Denote the number of muscle channels as C and $C = 16$ in this study, as mentioned in Section 3.1.

For the SVM model, input representations are constructed as follows:

- Raw sEMG signals: d commonly used time-frequency features (as described in Section 3.2) are extracted from each segment of each muscle channel, forming a feature matrix of size $L \times C \times d$.
- sEMG tokens: For each muscle, d' statistical features are computed over the entire token sequence of length L , yielding a $C \times d'$ feature matrix. d' statistical features include: token ratio (proportion of each token), token transition Frequency (frequency of token changes), token duration statistics (average and maximum continuous durations), and basic statistics (mean, variance, skewness, kurtosis). And $mean = \frac{1}{L} \sum_{i=1}^L s_i$; $variance = \frac{1}{L} \sum_{i=1}^L (s_i - mean)^2$; $skewness = \frac{\frac{1}{L} \sum_{i=1}^L (s_i - mean)^3}{(variance)^{3/2}}$; $kurtosis = \frac{\frac{1}{L} \sum_{i=1}^L (s_i - mean)^4}{(variance)^2} - 3$, where s_i is the token value at time step i .

Both feature matrices are flattened into one-dimensional vectors before being fed into the SVM classifier. This setup allows for a direct comparison between sEMG tokens derived from raw signals and statistical summaries.

For the ViT model, no explicit feature engineering is performed. The raw sEMG input consists of T sampling points from C muscle channels, structured as a $T \times C$ matrix, which is segmented into L windows. Similarly, the token-based input forms a $L \times C$ matrix, where each entry corresponds to a symbolic token representing the discretized muscle

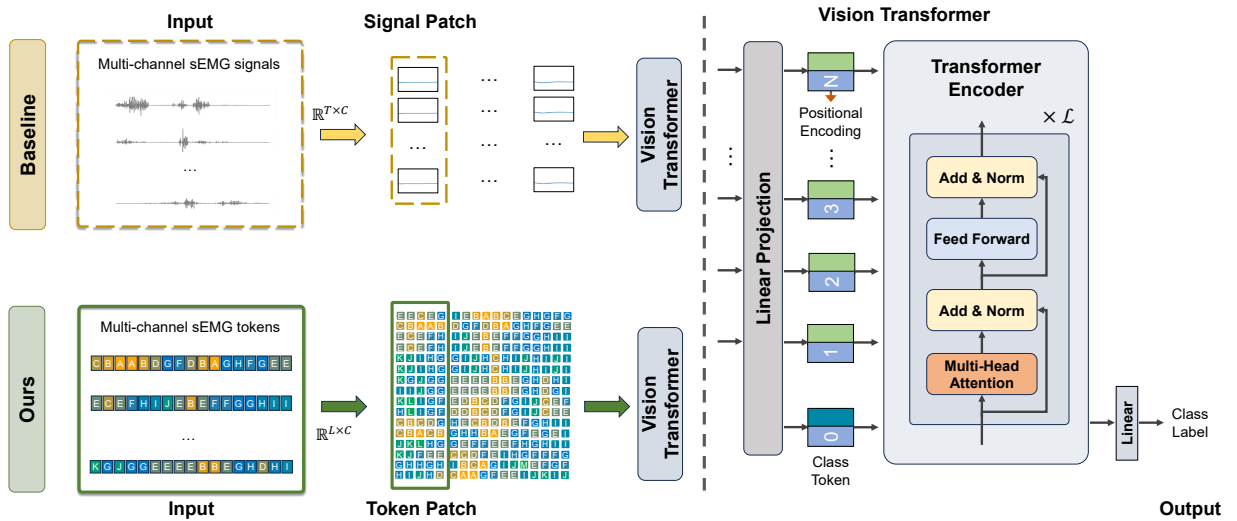


Figure 5: ViT-based human action recognition model. For 16 muscles, the input sequence is either the raw sEMG signals or the corresponding sEMG tokens sequence. The sequence is divided into several temporal patches. Each patch is passed through a linear projection and positional embedding layer, and a class token is added to the beginning of the sequence. The resulting sequence is then processed by the transformer encoder. Raw sEMG signals are smoothed using a first-order low-pass Butterworth filter before segmentation.

state over time. Both input types are processed using the same ViT backbone. Each input sequence is divided into temporal patches, which are then projected into a latent embedding space by a learnable linear layer. To aggregate global sequence information, a learnable class token $\mathbf{x}_{\text{cls}} \in \mathbb{R}^D$ is prepended to the sequence, where D is the model dimension. Positional encoding $\mathbf{E}_{\text{pos}} \in \mathbb{R}^{(P+1) \times D}$ is added to retain temporal order information. Here P is the number of patches and $P = 256$ and 8 for sEMG signals and tokens input respectively. Formally, the input to the Transformer encoder is:

$$\mathbf{Z}_0 = [\mathbf{x}_{\text{cls}}; \mathbf{x}_1; \mathbf{x}_2; \dots; \mathbf{x}_P] + \mathbf{E}_{\text{pos}}$$

where $\mathbf{x}_i \in \mathbb{R}^D$ is the embedding for the i -th patch.

The Transformer Encoder is composed of \mathcal{L} blocks. For the l -th block, given the input \mathbf{Z}_{l-1} , it is processed sequentially through a Multi-Head Attention (MHA) mechanism and a Feed-Forward Network (FFN), both followed by a residual connection and Layer Normalization (LayerNorm) (Ba et al., 2016):

$$\mathbf{Y}_l = \text{LayerNorm}(\mathbf{Z}_{l-1} + \text{MHA}(\mathbf{Z}_{l-1}))$$

$$\mathbf{Z}_l = \text{LayerNorm}(\mathbf{Y}_l + \text{FFN}(\mathbf{Y}_l))$$

where $\text{MHA}(\mathbf{Z}) = \text{Concat}(\text{head}_1, \dots, \text{head}_h) \mathbf{W}^O$, and each attention head is computed by $\text{head}_i = \text{softmax} \left(\frac{\mathbf{Q}_i \mathbf{K}_i^T}{\sqrt{d_k}} \right) \mathbf{V}_i$.

Through this architecture, the Transformer encoder effectively models both temporal dependencies within each muscle channel and inter-muscle relationships, enabling end-to-end action classification.

In our implementation, we set $L = 256$ and $T = [(L - 1) \times 25 \text{ ms} + 50 \text{ ms}] \times 1269 \text{ Hz} \approx 8192$. The value of T matches the temporal span of the sEMG tokens sequence ($L = 256$) under a 50 ms window with 25 ms overlap at a sampling rate of 1269 Hz, ensuring temporal alignment for fair comparison. Notably, the tokenized representation reduces the input dimension by approximately 96% compared to the raw sEMG signals (from $T \times C$ to $L \times C$). For the ViT model, D and \mathcal{L} are set to 64 and 1 respectively. All experiments are conducted using five-fold subject-wise cross-validation to ensure robustness and generalizability.

3.4.2. Quantification of Movement Quality

To evaluate movement quality, we reformulate the task as a sequence similarity problem between the subject's execution and the standard action provided by the fitness expert. Specifically, we use the MEQAD dataset, which

contains both correct and faulty executions of several actions. Since different subjects may vary in action duration and speed, we adopt Dynamic Time Warping (DTW) to align and compare sequences of differing lengths.

In our setup, each action is represented by a sequence of sEMG tokens reflecting the activation states of C muscles over time. Formally, each action sequence is denoted as:

$$S = \left[s_1^{(1)}, s_1^{(2)}, \dots, s_1^{(C)} \right], \left[s_2^{(1)}, s_2^{(2)}, \dots, s_2^{(C)} \right], \dots, \left[s_T^{(1)}, s_T^{(2)}, \dots, s_T^{(C)} \right] \quad (6)$$

where $s_i^{(m)}$ is the token value of the m -th muscle at time step i , with T representing the total number of time steps.

To compare two sequences S^A and S^B , we define the pointwise distance between time steps i and j as the L1 norm across all muscle channels. The DTW distance is then computed recursively via dynamic programming:

$$D(i, j) = L1(S_i^A, S_j^B) + \min(D(i-1, j-1), D(i-1, j), D(i, j-1)) \quad (7)$$

where $D(i, j)$ denotes the cumulative alignment cost between the first i steps of sequence A and the first j steps of sequence B .

The final DTW distance $\text{DTW}(S^A, S^B) = D(L_A, L_B)$, where L_A, L_B are the sequence lengths. It provides a temporal alignment score that reflects the overall similarity in muscle activation patterns between two executions. Despite its simplicity, this distance metric captures both timing and pattern differences in a compact form.

To translate the DTW distance into an interpretable quality score, we follow the method in (Yu and Xiong, 2019) and compute:

$$\text{Similarity Score} = 1 - \frac{\text{DTW}(S^A, S^B)}{\text{Max}_{\text{error}} \times C \times \hat{L}} \quad (8)$$

Here, $\text{Max}_{\text{error}}$ denotes the maximum possible token difference (e.g., from rest to maximal contraction), which equals $K - 1$ in our setting. \hat{L} is the length of the optimal warping path. The resulting score ranges from 0 to 100%, with higher values indicating greater similarity to the standard execution.

This approach provides a simple yet effective means of quantifying movement quality based on tokenized sEMG sequences.

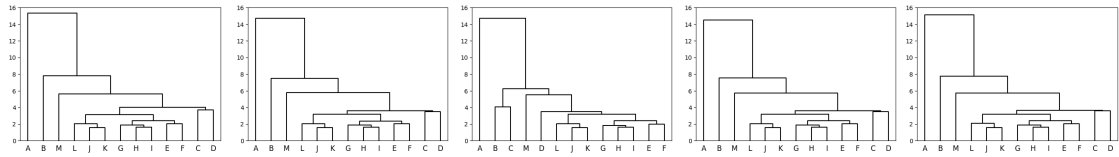
4. Results

4.1. Physiological Semantics of sEMG Tokens

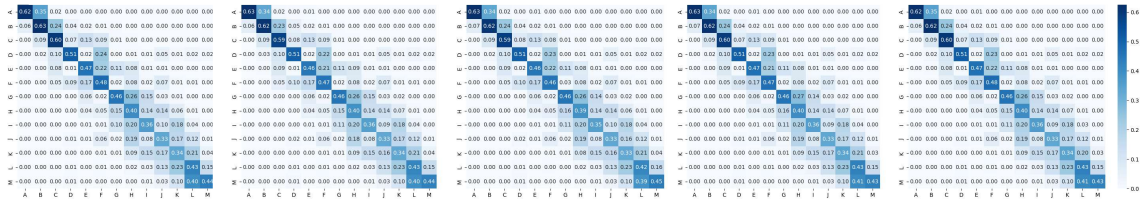
To systematically encode muscle activation dynamics in a compact and interpretable form, raw sEMG signals are segmented using a fixed-length sliding window, where the window length is matched to the minimal muscle contraction cycle. This ensures that each segment represents discrete muscle activation information without excessive fragmentation or overlap between multiple contraction cycles. From each segment, a set of ten commonly utilized features is extracted to characterize both time-domain properties (e.g., RMS, MAV, WL) and frequency-domain attributes (e.g., MDF, MNF), capturing key aspects of local muscle activity. The resulting feature vectors are then clustered using the K-means algorithm, with each cluster centroid corresponding to a distinct muscle state token. This tokenization process transforms continuous sEMG signals into symbolic sequences that encapsulate representative patterns of muscle activation. Details of the tokenization procedure are provided in Section 3.2.

Since transitions between muscle activation states typically occur in a gradual and continuous manner, we hypothesize that the generated sEMG tokens sequences exhibit an intrinsic organization across both their feature space and temporal sequence. To validate this hypothesis, hierarchical clustering is employed to analyze the relationships among tokens within the feature space, capturing their similarity in underlying muscle activation patterns. The hierarchical clustering results (Fig 6-A) reveals that sEMG tokens form a structured feature space, where tokens with similar muscle activation states cluster together, reflecting physiologically meaningful spatial distances. Additionally, token-level transition probability matrices are constructed to reveal sequential co-occurrence patterns in the temporal domain. By integrating these feature-space relationships and temporal dynamics, we derive an ordered structure of sEMG tokens that aligns with physiologically plausible muscle activation transitions. As shown in Fig 6-B, results from five-fold cross-validation consistently demonstrate that tokens associated with adjacent time windows follow coherent transition trajectories, aligning with the progressive nature of muscle activation. This structured representation not only

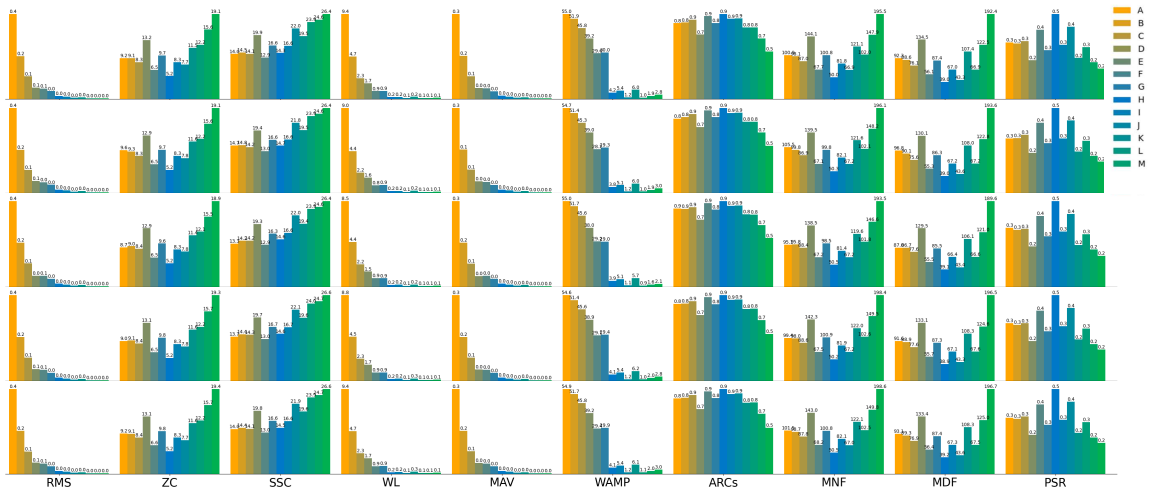
A. Feature Space: Hierarchical Clustering of sEMG Tokens



B. Temporal Dynamics: State Transition Matrix



C. Time-Frequency Features of Clustering Centroids



D. Time-Frequency Comparison between Token A and Token M

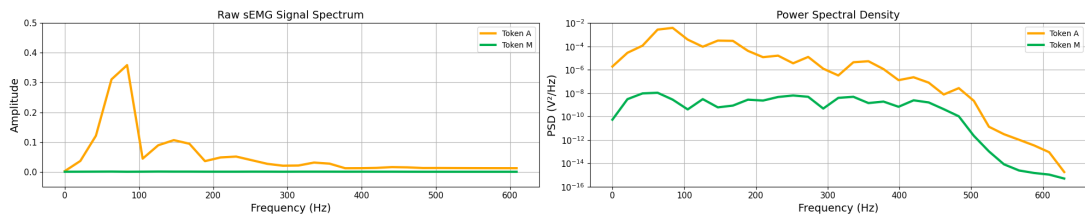


Figure 6: Physiological semantics of sEMG tokens. (A) Hierarchical clustering of token feature vectors across five folds reveals consistent spatial proximity across folds. (B) Token transition matrices across five folds highlight the progressive and ordered nature of token sequences. (C) Distribution of cluster centroid features across folds reflects consistent encoding of muscle activation states. (D) Power spectral comparison between token A and token M illustrates clear physiological contrasts.

enhances the interpretability of token sequences but also provides a meaningful symbolic foundation for downstream applications such as action classification and movement quality assessment.

We present the feature vectors of the cluster centroids in Fig 6-C to investigate the physiological interpretability of the generated sEMG tokens. Notably, across all five-fold cross-validation experiments, token A consistently exhibits significantly elevated values across several representative time-domain features (e.g., RMS, WL, MAV, WAMP), all of which are widely used indicators of muscle contraction intensity. This distinct feature pattern suggests that token A encodes a high-activation state. According to the motor unit recruitment theory (Henneman's size principle)

(Henneman et al., 1965; Farina et al., 2014), stronger muscle contractions involve the recruitment of larger and more numerous motor units, which in turn manifest as higher amplitudes in sEMG signals. Therefore, we infer that token A corresponds to a state of strong muscle contraction, likely reflecting periods of active effort or peak activation.

In contrast, token M shows the lowest values across the aforementioned time-domain features, characterized by low amplitude and stable signal fluctuations. Further frequency-domain analysis reveals a relatively uniform power spectral distribution across the entire frequency band. Specifically, as illustrated in Fig 6-D, the spectral energy of token A is concentrated around 100 Hz, whereas token M exhibits a flatter spectral profile approaching the baseline noise level of the recording equipment (Boyer et al., 2023; De Luca et al., 2010). These findings suggest that token M likely corresponds to a resting muscle state or a period of minimal activation.

These findings indicate that token M represents a resting or minimally activated muscle state, while token A corresponds to strong muscle contraction. Importantly, intermediate tokens capture physiologically meaningful states that lie between these extremes, reflecting gradual transitions in muscle activation intensity.

4.2. Inter-subject Consistency of sEMG Tokens

Although the sEMG tokens are derived from training data involving a limited number of individuals, our framework is designed to capture fundamental patterns of muscle activation that generalize beyond specific subjects. To verify this, we conduct an inter-subject consistency analysis to evaluate whether the token representation remains stable across different individuals.

We assess token stability using a label consistency experiment that compares two token generation strategies. In the first strategy, token assignments are obtained by applying a clustering model trained on the training set (Fig. 7-A). In the second, clustering is independently performed on the test set (Fig. 7-B). The consistency between these two strategies is measured at the token-label level. We conduct five-fold cross-validation with subject-wise data partitioning. In each fold, token labels derived from the training-set model are compared to those obtained from clustering on the test set. Token-level confusion matrices across all folds are presented in Fig. 7-C. With a 13-token configuration, the token label overlap rates across the five folds were 75.5%, 92.6%, 87.8%, 91.8%, and 71.2%, yielding an average of $83.78\% \pm 8.80\%$. Corresponding Cohen's Kappa scores were 0.73, 0.92, 0.87, 0.91, and 0.68, with a mean of 0.82 ± 0.09 . These results demonstrate that the proposed sEMG tokens representation exhibits strong consistency across subjects, supporting its robustness and generalizability.

Recognizing that real-world muscle activations evolve gradually and often lack sharply defined boundaries, we further introduce a tolerance-aware consistency metric. Under this relaxed criterion, two token labels are considered consistent if their difference is within ± 1 . Using this approach, the average agreement rate increases to $90.00\% \pm 5.96\%$, underscoring the stability of the sEMG tokens even under semantically flexible conditions.

4.3. Representation Capacity of sEMG Tokens

The proposed tokenization framework compresses continuous, high-dimensional sEMG signals into discrete tokens while preserving essential physiological information. Despite substantial dimensionality reduction, the sEMG tokens retain strong discriminative power for representing human muscle dynamics.

To compare the representation capacity of sEMG tokens with that of raw sEMG signals, we evaluate their performance on action recognition using Support Vector Machine (SVM) and Vision Transformer (ViT) respectively. All experiments are conducted under the subject-wise five-fold cross-validation protocol. As shown in Table 2, sEMG tokens consistently outperform raw signals across standard classification metrics. In the SVM setting, sEMG tokens increase Top-1 accuracy from 64.4% to 67.9% and macro-averaged F1-score from 61.5% to 67.8% compared to raw signals. In the ViT model, sEMG tokens improve Top-1 accuracy from 72.8% to 75.5% and F1-score from 69.3% to 72.4%, while reducing input dimensionality by 96%. These results demonstrate that the tokenized representation effectively retains the key information required for accurate action recognition. Notably, these experiments adopt a cross-subject setting, where training and test data come from different individuals. The consistent improvements demonstrate that sEMG tokens capture subject-independent features of muscle activation, offering greater robustness than raw signals, which are highly sensitive to individual variability.

Further analysis of confusion matrices (Fig. 8) reveals that sEMG tokens reduce misclassifications between actions with distinct muscle activation patterns. For instance, the confusion between Single-Leg Stand (class 26) and Sit Up (class 6) decreases by 18 cases, and between Standing External Hip Rotation (class 42) and Jogging (class 0) by 11 cases. This indicates that the token representation more accurately captures and expresses the primary muscle activation patterns of different actions, thereby enhancing the model's ability to distinguish between them. However, they also

A. sEMG Tokens Inferred from Train Set

B. sEMG Tokens Clustered on Test Set



C. Inter-subject Consistency of sEMG Tokens Evaluated via 5-Fold Cross-Validation

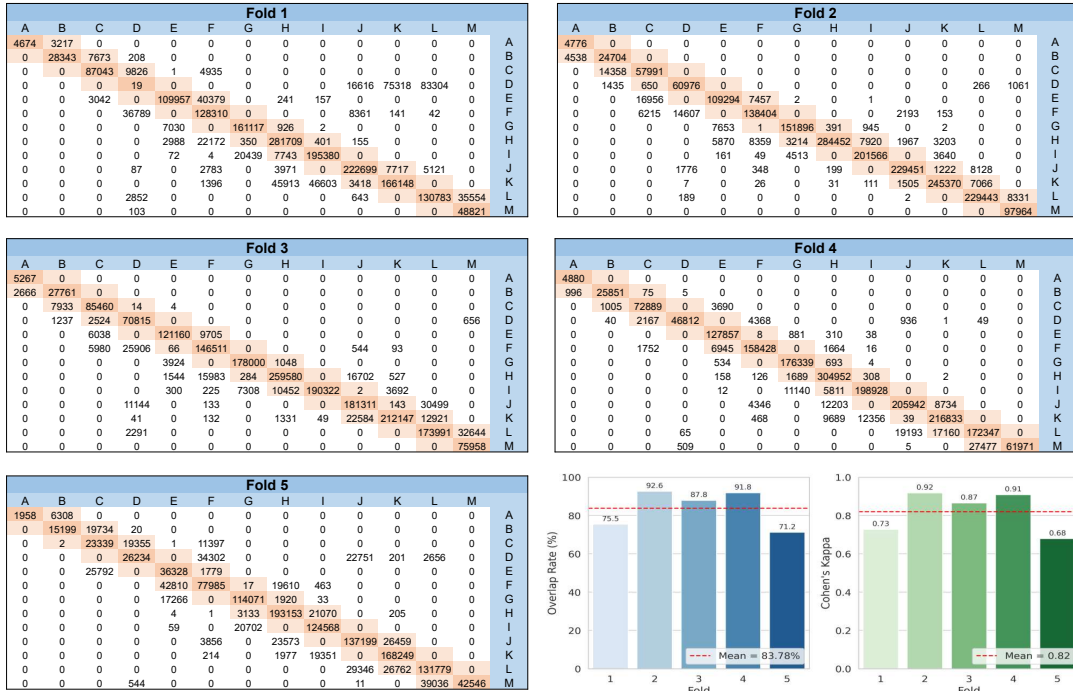


Figure 7: Consistency analysis of the proposed sEMG tokens. (A) represents the sEMG tokens inferred from the train set, while (B) represents the sEMG tokens obtained by independent clustering on the test set. C shows the confusion matrices calculated based on five-fold cross-validation, used to evaluate the consistency between the two strategies at the token label level. In the confusion matrix, columns correspond to strategy A, and rows correspond to strategy B. Overall, the high overlap rate between the two strategies in label assignment ($83.78 \pm 8.80\%$) and the relatively high Cohen's Kappa (0.82 ± 0.09).

introduce some new misclassifications, mainly between actions with highly similar muscle activation patterns. For instance, misclassifications between Horse Stance (class 28) and Squats (class 4), or Bounding (class 32) and Lunge Jumps (class 25), increase modestly. These confusions are expected, as such actions inherently involve overlapping activation in both timing and intensity across similar muscle groups.

Overall, sEMG tokens efficiently extract and emphasize the primary muscle activation features of actions, significantly reducing confusion between actions with markedly different activation patterns. Although they introduce some difficulty in distinguishing actions with highly similar muscle activation modes, this precisely reflects the token's focus on primary features. Taken together, these results strongly demonstrate that sEMG tokens, as an efficient feature representation method, have a significant advantage in capturing the essential muscle dynamics of actions, offering a new approach to improving fine-grained action recognition based on sEMG.

Table 2
Experimental results of sEMG-based human action recognition

SVM	-	Top-1	Top-3	P(macro)	R(macro)	F1(macro)
sEMG signals	Fold 1	0.5736	0.7756	0.6222	0.5719	0.5519
	Fold 2	0.6599	0.8426	0.6479	0.6183	0.6002
	Fold 3	0.6190	0.8179	0.7077	0.6345	0.6263
	Fold 4	0.6944	0.8464	0.7285	0.6887	0.6768
	Fold 5	0.6733	0.8564	0.6672	0.6338	0.6186
	Mean	0.6440	0.8278	0.6747	0.6294	0.6148
sEMG tokens	Fold 1	0.6330	0.8380	0.6623	0.6372	0.6207
	Fold 2	0.7208	0.9154	0.7357	0.7228	0.7098
	Fold 3	0.6457	0.8754	0.6978	0.6965	0.6761
	Fold 4	0.6928	0.8848	0.7176	0.6885	0.6762
	Fold 5	0.7030	0.9431	0.7807	0.7212	0.7080
	Mean	0.6790	0.8913	0.7188	0.6933	0.6782
ViT	-	Top-1	Top-3	P(macro)	R(macro)	F1(macro)
sEMG signals	Fold 1	0.7637	0.9227	0.7865	0.7352	0.7260
	Fold 2	0.7411	0.9137	0.7163	0.7274	0.6977
	Fold 3	0.6919	0.8711	0.7405	0.6789	0.6712
	Fold 4	0.7168	0.9328	0.7504	0.7046	0.7010
	Fold 5	0.7252	0.8886	0.7086	0.6964	0.6670
	Mean	0.7278	0.9058	0.7405	0.7085	0.6926
sEMG tokens	Fold 1	0.7266	0.8767	0.7076	0.7069	0.6911
	Fold 2	0.7902	0.8934	0.7991	0.7736	0.7678
	Fold 3	0.7297	0.9244	0.7780	0.7243	0.7229
	Fold 4	0.7536	0.9104	0.7720	0.7378	0.7239
	Fold 5	0.7748	0.8960	0.7535	0.7504	0.7161
	Mean	0.7550	0.9002	0.7620	0.7386	0.7244

4.4. Interpretability of sEMG Tokens

The proposed sEMG tokens offer strong interpretability by discretizing continuous, noisy, and high-dimensional signals into a compact set of symbolic states, each corresponding to a distinct muscle activation level. This transformation preserves essential physiological information while abstracting away subject-specific noise, yielding a structured representation more aligned with human understanding of muscle dynamics. To validate the practical utility of this interpretability, we apply sEMG tokens to movement quality assessment, a task that demands fine-grained insight into execution differences within the same action class.

We first conduct an intra-subject analysis using data from a certified fitness expert. For each target action (High Knees, Squats, and Biceps Curl), the expert performed both correct and deliberately faulty executions, with the latter incorporating common deviations such as muscle underactivation or compensatory recruitment. The correct executions serve as the standard samples. To evaluate execution consistency and deviations, we calculate the average Dynamic Time Warping (DTW) similarity both among the standard executions and between faulty and standard samples. This comparison is performed from two perspectives: All Muscles and Primary Muscles, the latter focusing on muscles most responsible for the target action and most sensitive to execution errors. As shown in Table 3, the sEMG tokens reveal a clear hierarchical structure in capturing execution quality. For example, in the Biceps Curl, average DTW similarity within standard executions reaches 0.914 (All Muscles) and 0.931 (Primary Muscles), while similarity between faulty and standard executions decreases to 0.895 and 0.859, respectively. The clear drop in DTW similarity, captured by this simple metric, shows that the tokens effectively represent subtle differences in muscle activation, such as compensatory deltoid involvement. The definition of Primary Muscles for actions is provided in Table 6.

We also conduct a cross-subject analysis using data from two untrained participants who performed both standard and faulty executions under expert instruction. As shown in Table 4, the results consistently exhibit a clear hierarchical pattern. For High Knees, the average DTW similarity between correct executions and the expert's standard samples (on

A. Confusion Matrix of sEMG Signals

B. Confusion Matrix of sEMG Tokens

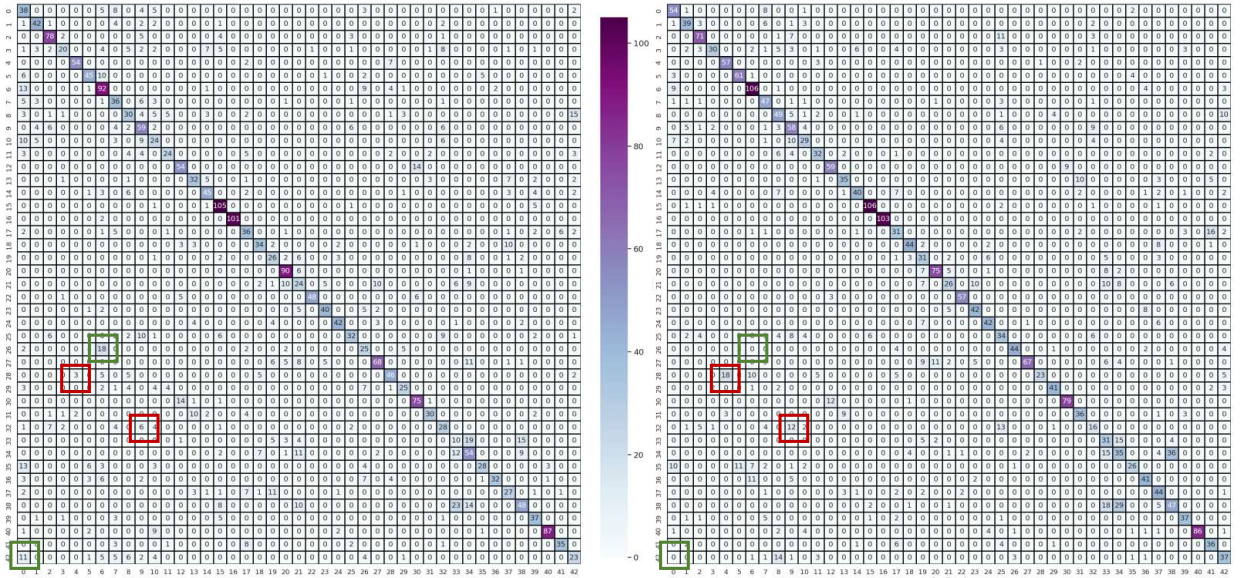


Figure 8: The aggregated confusion matrices of the SVM model across five-fold cross-validation. (A) shows the confusion matrix based on raw sEMG signals; (B) shows the confusion matrix based on sEMG tokens. In each confusion matrix, the vertical axis represents the ground truth labels and the horizontal axis represents the predicted labels. The action labels correspond to all indices are provided in Appendix Table. 5. Green boxes highlight several misclassifications corrected by the sEMG tokens, while red boxes indicate some new misclassifications introduced by the token-based method.

Table 3

Intra-subject comparison of average DTW similarity between correct and faulty executions using sEMG tokens, based on data from a certified fitness expert. Similarity is calculated among correct samples and between faulty and correct samples, from both *All Muscles* and *Primary Muscles* perspectives.

		All Muscles	Primary Muscles
High Knees	standard vs. standard	0.900±0.000	0.900±0.000
	faulty vs. standard	0.865±0.000	0.870±0.006
Squats	standard vs. standard	0.907±0.002	0.942±0.003
	faulty vs. standard	0.883±0.002	0.903±0.005
Bicep Curl	standard vs. standard	0.914±0.001	0.931±0.002
	faulty vs. standard	0.895±0.001	0.859±0.002

primary muscles) is 0.863, dropping to 0.793 for faulty executions. In Biceps Curl, the similarity scores similarly drop from 0.918 (correct vs. standard) to 0.770 (faulty vs. standard). These results indicate that the sEMG tokens effectively capture differences in execution quality across individuals, with strong sensitivity to deviations in key muscle groups.

We further present a qualitative analysis based on two representative case studies. Figure 9-A illustrates the sEMG tokens of an ordinary subject when correctly performing the Biceps Curl. The participant’s sEMG tokens sequence closely aligns with that of the expert, particularly highlighting strong activation in the biceps brachii. In contrast, during the faulty execution in Figure 9-B, which involves elbow elevation and compensatory activation, the token sequence exhibits a noticeable increase in deltoid activity, revealing the presence of undesired muscle compensation. This example illustrates how the tokenized representation alone can reveal subtle but physiologically meaningful deviations in muscle recruitment.

In summary, the proposed sEMG tokens provide a structured and physiologically grounded representation of muscle states that enhances interpretability. Through both quantitative and qualitative analyses, we demonstrate that these tokens can sensitively distinguish between correct and faulty executions, particularly in primary muscles

Table 4

Cross-subject comparison of average DTW similarity between ordinary participants' executions and template samples using sEMG tokens. Each participant performs both correct and faulty versions under expert instruction. *Template* refers to the expert's correct executions.

		All Muscles	Primary Muscles
High Knees	correct vs. standard	0.835±0.003	0.863±0.004
	faulty vs. standard	0.820±0.001	0.793±0.003
Squats	correct vs. standard	0.855±0.003	0.905±0.002
	faulty vs. standard	0.841±0.004	0.883±0.006
Bicep Curl	correct vs. standard	0.859±0.001	0.918±0.001
	faulty vs. standard	0.816±0.001	0.770±0.005

where deviations are most informative. The qualitative visualizations further support this interpretability by revealing token-level differences in specific muscle regions (e.g., deltoid compensation during faulty biceps curls), offering intuitive insights into muscle activation dynamics. These results establish sEMG tokens as a compact and transparent representation well-suited for personalized feedback and rehabilitation applications.

5. Discussion

This study presents a fundamentally new perspective on the analysis of sEMG signals by recasting continuous biosignals into discrete, physiologically interpretable tokens. Traditional sEMG analysis methods predominantly focus on modeling raw signal waveforms or extracting handcrafted features, which often suffer from limited robustness and poor generalizability due to inherent noise and inter-subject variability. In contrast, our tokenization framework prioritizes the extraction of semantically meaningful muscle activation states, aligning computational representations more closely with the underlying physiological processes.

The proposed sEMG tokens exhibit three key advantages: inter-subject consistency, representation capacity, and interpretability. First, the tokenization process shows strong inter-subject consistency. Token labels inferred from independent clustering procedures align closely across individuals (Cohen's Kappa = 0.82, overlap = 83.8%), suggesting that the tokens capture invariant and transferable muscle activation patterns. Second, in action recognition, the tokens outperform raw signals across multiple metrics despite reducing signal dimensionality by over 96%, confirming that essential movement-related information is preserved. Third, the symbolic structure of the tokens significantly enhances interpretability. In movement quality assessment, a simple similarity metric, DTW, is sufficient to reveal subtle deviations in execution quality, such as muscle underactivation or undesired compensation. This demonstrates the clarity and utility of the learned representation in practical scenarios.

A limitation of this study lies in the dataset scale. Although ActionEMG-43 provides a diverse set of 43 full-body actions, it is constructed from only 14 participants. While we demonstrate promising performance and generalization within this cohort, broader validation is necessary to assess robustness across larger, more heterogeneous populations, including varying ages, fitness levels, and clinical conditions.

Future work may expand the tokenization framework by collecting larger and more demographically diverse datasets, enabling broader generalization and personalization. Integrating additional sensing modalities (e.g., inertial or kinematic data) and exploring sequence modeling techniques over token streams may also enhance performance in downstream tasks such as rehabilitation monitoring, motor learning, and human-machine interaction. As a compact, structured, and physiologically meaningful representation, sEMG tokens offer a promising foundation for interpretable and scalable muscle analysis in both research and applied settings.

6. Conclusion

This work introduces a novel tokenization framework for sEMG signals, providing a structured and interpretable representation of muscle activation states. In contrast to traditional methods that focus on reconstructing continuous biosignals, our approach emphasizes the extraction of semantically meaningful and compact representations, which are more robust to inter-subject variability and more suitable for downstream applications. Through extensive experiments on human action recognition and movement quality assessment, we demonstrate that sEMG tokens exhibit strong representation capacity, inter-subject consistency, and physiological interpretability. These properties not only enable

A. Correct Biceps Curl Execution VS. Standard



B. Faulty Biceps Curl Execution VS. Standard

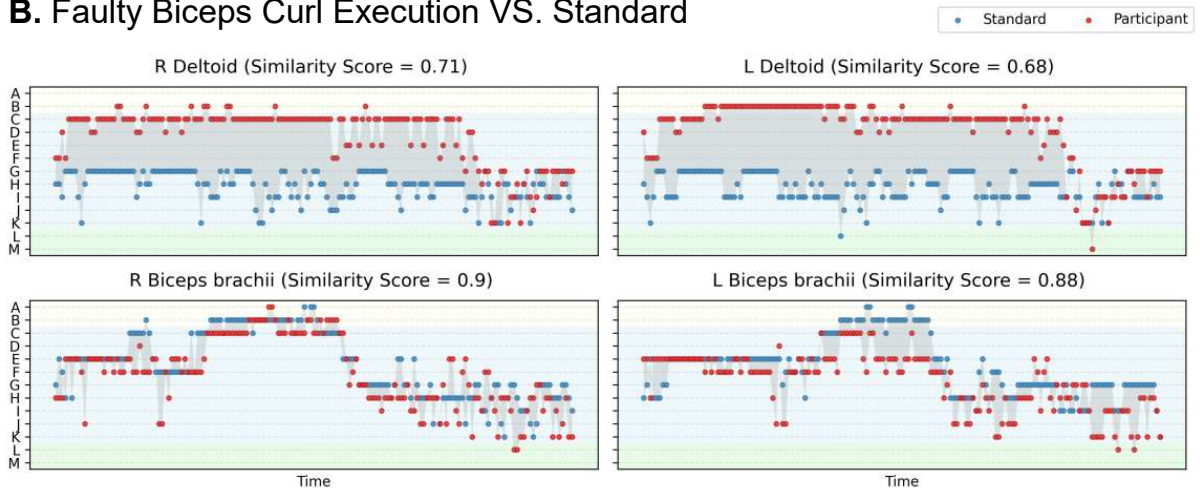


Figure 9: Comparison on sEMG tokens between participant's Biceps Curl with standard execution. Blue points represent the sEMG tokens sequence of the standard execution provided by the fitness expert, while red points indicate the sEMG tokens sequence of an ordinary participant. The shaded regions highlight the discrepancies between the two token sequences, revealing differences in muscle activation states. For visual clarity, this figure focuses on the deltoid and biceps brachii muscles. Full comparisons across all muscle groups are provided in Appendix Fig. 10.

competitive performance in classification tasks but also facilitate fine-grained analysis of execution quality using lightweight similarity metrics. Overall, this study offers a promising direction for building scalable, explainable, and task-aware muscle-computer interfaces, with potential applications in personalized training, rehabilitation, and human-machine interaction.

CRedit authorship contribution statement

Yuepeng Chen: Conceptualization, Methodology, Writing – original draft. **Kaili Zheng:** Writing–review&editing, Validation, Methodology. **Ji Wu:** Supervision, Writing–review&editing. **Zhuangzhuang Li:** Data curation, Investigation. **Ye Ma:** Methodology, Formal analysis. **Dongwei Liu:** Methodology, Formal analysis. **Chenyi Guo:** Supervision, Writing–review&editing. **Xiangling Fu:** Supervision, Writing–review&editing.

Declaration of competing interest

The authors declare no competing interests. The authors declare that they have no known competing financial interests or personal relationships that could have appeared to influence the work reported in this paper.

Data availability

The ActionEMG-43 dataset used in this study is currently available from the corresponding author on reasonable request. The dataset will be released publicly after the manuscript is accepted for publication, to support reproducibility and further research.

Acknowledgments

This work was supported by the Tsinghua University Initiative Scientific Research Program and the Natural Science Foundation of Beijing(Grant No.L242049).

Ethics

This study was approved by the Institutional Review Board of Tsinghua University (Approval No. THU01-20240069). All the data was totally de-identified to ensure con-fidentiality and privacy.

A. Appendix

A.1. Dataset Description

The ActionEMG-43 dataset contains 43 distinct human actions commonly involved in physical training, rehabilitation, and daily movement tasks. A detailed list of all action classes is presented in Table. 5.

In addition to general actions, we constructed an Movement Quality Evaluation Dataset consisting of representative exercises, each with a well-defined standard execution template and a common error variant. To facilitate objective evaluation, we analyzed muscle activation differences between correct and incorrect executions. Table. 6 summarizes the key characteristics of three representative actions, including definitions, error descriptions, and associated changes in muscle activity.

Table 5
Action Categories in the ActionEMG-43 Dataset

ID	Action Name	ID	Action Name
0	Jogging	22	Plank with Alternating Arm Raise
1	High Knees	23	Standing Head Turn to Look at Object
2	Frog Jumps	24	Maximal Forward Reach with One Arm Fist Clench
3	High Kicks	25	Lunge Jumps
4	Squats	26	Single-Leg Stand
5	Walking with Turning	27	Biceps Curl
6	Sit Up	28	Horse Stance
7	Butt Kicks	29	Alternating Box Jumps
8	Side Kick	30	V-Up
9	Fast Feet with Arm Swing and Squat	31	Straight Leg Lunge
10	Foot Fire	32	Bounding
11	Lateral Lunge	33	Arm Circles
12	Quadruped Bridge	34	Lat Pulldown without Equipment
13	Hurdle Steps	35	Brisk Walking
14	Side Leg Swings	36	Forward Bend to Pick Up Object
15	Jumping Jacks	37	Heel-to-Glute with Arm Reach
16	Seated Toe Raises	38	Standing Overhead Press without Equipment
17	Walking Lunge with Trunk Rotation	39	Cross Steps
18	Abdominal and Back Stretch	40	Calf raises
19	Standing Side Bend	41	Standing Front Press without Equipment
20	Bent Over T-Raises	42	Standing External Hip Rotation
21	Standing Head-Hand Resistance Stretch		

Table 6
Movement Quality Assessment Dataset

Action Name	Standard Action Definition	Error Action Description	Primary Muscle Activation Differences
High Knees	Performed with forefoot landing , upright and stable torso, and consistent rhythm throughout the motion.	Whole foot lands flat, indicating insufficient lower limb muscle activation and reduced body control.	Due to the shift from forefoot to flat-foot contact, the activation intensity of the gastrocnemius is significantly reduced.
Squats	Torso leans forward moderately, coordinated hip and knee flexion, heel firmly planted, and center of gravity maintained posteriorly.	Limited ankle dorsiflexion leads to heel lift, shifting the center of gravity forward and compromising balance.	The gastrocnemius shows compensatory overactivation due to poor ankle mobility.
Biceps Curl	Elbows remain close to the torso, with movement driven primarily by contraction of the biceps brachii .	Compensatory shoulder flexion causes forward movement of the upper arm, disrupting the intended trajectory.	Significant increase in activation of the anterior deltoid , reflecting excessive involvement of non-target muscles

A.2. Case Study: sEMG Tokens Analysis of Biceps Curl Across All Muscles

To extend the qualitative findings in the main text, this appendix presents additional sEMG tokens comparisons across all recorded muscle groups. Figures 10 illustrate the token trajectories of both the fitness expert and the ordinary participant during a single biceps curl execution. These visualizations reveal muscle-specific deviations, such as compensatory activation in non-target muscles like the deltoid or insufficient recruitment of primary movers, which are often difficult to detect in raw sEMG signals. By capturing physiologically meaningful discrepancies, the tokenized representation provides a structured and interpretable perspective on inter-muscle coordination, enabling a more comprehensive assessment of execution quality.

A. Correct Biceps Curl Execution VS. Standard



B. Faulty Biceps Curl Execution VS. Standard



Figure 10: sEMG Tokens-Based Comparison between Ordinary Individuals' Biceps Curl Execution and Expert-Level Performance. Blue points represent the sEMG tokens transitions of the fitness expert during a single execution, while red points indicate the sEMG tokens transitions of the ordinary participant during a single execution. The shaded regions highlight the discrepancies between the two token sequences, revealing differences in muscle activation states.

References

- Ait Yous, M., Agounad, S., Elbaz, S., 2025. Detection, identification and removing of artifacts from semg signals: Current studies and future challenges. *Computers in Biology and Medicine* 186, 109651. URL: <https://www.sciencedirect.com/science/article/pii/S0010482525000010>, doi:<https://doi.org/10.1016/j.combiomed.2025.109651>.
- Atzori, M., Gijssberts, A., Castellini, C., Caputo, B., Hager, A.G.M., Elsig, S., Giatsidis, G., Bassetto, F., Müller, H., 2014. Electromyography data for non-invasive naturally-controlled robotic hand prostheses. *Scientific data* 1, 1–13.
- Ba, J.L., Kiro, J.R., Hinton, G.E., 2016. Layer normalization. *arXiv preprint arXiv:1607.06450*.
- Barona López, L.I., Ferri, F.M., Zea, J., Ángel Leonardo Valdivieso Caraguay, Benalcázar, M.E., 2024. Cnn-lstm and post-processing for emg-based hand gesture recognition. *Intelligent Systems with Applications* 22, 200352. URL: <https://www.sciencedirect.com/science/article/pii/S2667305324000280>, doi:<https://doi.org/10.1016/j.iswa.2024.200352>.
- Bezrukov, V.A., Vakhtov, R.R., Chuykin, S.A., Anuchin, P.Y., Siziakova, A.Y., 2024. Evaluating the accuracy of knn classifier for gesture detection based on forearm emg signal, in: *2024 6th International Youth Conference on Radio Electronics, Electrical and Power Engineering (REEPE)*, pp. 1–5. doi:10.1109/REEPE60449.2024.10479744.
- Bittibssi, T.M., Genedy, M.A., Maged, S.A., et al., 2021. semg pattern recognition based on recurrent neural network. *Biomedical signal processing and control* 70, 103048.
- Bonato, P., Boissy, P., Della Croce, U., Roy, S.H., 2002. Changes in the surface emg signal and the biomechanics of motion during a repetitive lifting task. *IEEE Transactions on Neural Systems and Rehabilitation Engineering* 10, 38–47.

- Borsos, Z., Marinier, R., Vincent, D., Kharitonov, E., Pietquin, O., Sharifi, M., Roblek, D., Teboul, O., Grangier, D., Tagliasacchi, M., et al., 2023. Audiolm: a language modeling approach to audio generation. *IEEE/ACM transactions on audio, speech, and language processing* 31, 2523–2533.
- Boudreau, S.N., Dwyer, M.K., Mattacola, C.G., Lattermann, C., Uhl, T.L., McKeon, J.M., 2009. Hip-muscle activation during the lunge, single-leg squat, and step-up-and-over exercises. *Journal of sport rehabilitation* 18, 91–103.
- Boyer, M., Bouyer, L., Roy, J.S., Campeau-Lecours, A., 2023. Reducing noise, artifacts and interference in single-channel emg signals: A review. *Sensors* 23, 2927.
- Carlson, B.M., 2018. *The human body: linking structure and function*. Academic Press.
- Chen, W., Feng, L., Lu, J., Wu, B., Liu, D., 2023. Myobit: A public dataset based on an armband with 16 semg channels for gesture recognition under non-ideal conditions, in: 2023 27th International Conference on Methods and Models in Automation and Robotics (MMAR), pp. 69–74. doi:10.1109/MMAR58394.2023.10242547.
- Cifrek, M., Medved, V., Tonković, S., Ostojić, S., 2009. Surface emg based muscle fatigue evaluation in biomechanics. *Clinical biomechanics* 24, 327–340.
- Côté-Allard, U., Fall, C.L., Campeau-Lecours, A., Gosselin, C., Laviolette, F., Gosselin, B., 2017. Transfer learning for semg hand gestures recognition using convolutional neural networks, in: 2017 IEEE international conference on systems, man, and cybernetics (SMC), IEEE. pp. 1663–1668.
- Cvetković, S., Mišić, N., Ostojić, M., 2024. Modified spectral subtraction method to reduce noise in semg respiratory muscle signals, in: 2024 23rd International Symposium INFOTEH-JAHORINA (INFOTEH), IEEE. pp. 1–6.
- Day, S.J., Hulliger, M., 2001. Experimental simulation of cat electromyogram: evidence for algebraic summation of motor-unit action-potential trains. *Journal of Neurophysiology* 86, 2144–2158.
- De Luca, C.J., Donald Gilmore, L., Kuznetsov, M., Roy, S.H., 2010. Filtering the surface emg signal: Movement artifact and baseline noise contamination. *Journal of Biomechanics* 43, 1573–1579. URL: <https://www.sciencedirect.com/science/article/pii/S0021929010000631>, doi:<https://doi.org/10.1016/j.jbiomech.2010.01.027>.
- Défossez, A., Copet, J., Synnaeve, G., Adi, Y., 2022. High fidelity neural audio compression. arXiv preprint arXiv:2210.13438.
- Delph, M.A., Fischer, S.A., Gauthier, P.W., Luna, C.H.M., Clancy, E.A., Fischer, G.S., 2013. A soft robotic exomusculature glove with integrated semg sensing for hand rehabilitation, in: 2013 IEEE 13th International Conference on Rehabilitation Robotics (ICORR), IEEE. pp. 1–7.
- Disselhorst-Klug, C., Schmitz-Rode, T., Rau, G., 2009. Surface electromyography and muscle force: Limits in semg–force relationship and new approaches for applications. *Clinical biomechanics* 24, 225–235.
- Disselhorst-Klug, C., Williams, S., 2020. Surface electromyography meets biomechanics: correct interpretation of semg-signals in neuro-rehabilitation needs biomechanical input. *Frontiers in neurology* 11, 603550.
- Douglas, F., Pei, M., Kuo, C., 2025. Characterizing semg feature errors in lower limb muscles due to electrode location and skinelectrode interface changes. *IEEE Transactions on Instrumentation and Measurement*, 1–1doi:10.1109/TIM.2025.3568954.
- Duan, S., Wu, L., Xue, B., Liu, A., Qian, R., Chen, X., 2023. A hybrid multimodal fusion framework for semg-acc-based hand gesture recognition. *IEEE Sensors Journal* 23, 2773–2782.
- Fan, J., Jiang, M., Lin, C., Li, G., Fiaidhi, J., Ma, C., Wu, W., 2023. Improving semg-based motion intention recognition for upper-limb amputees using transfer learning. *Neural Computing and Applications* 35, 16101–16111.
- Farina, D., Merletti, R., Enoka, R.M., 2014. The extraction of neural strategies from the surface emg: an update. *Journal of applied physiology* 117, 1215–1230.
- Fratti, R., Marini, N., Atzori, M., Müller, H., Tiengo, C., Bassetto, F., 2024. A multi-scale cnn for transfer learning in semg-based hand gesture recognition for prosthetic devices. *Sensors* 24. URL: <https://www.mdpi.com/1424-8220/24/22/7147>.
- Frigo, C., Crenna, P., 2009. Multichannel semg in clinical gait analysis: a review and state-of-the-art. *Clinical Biomechanics* 24, 236–245.
- Fritsche, O., Camacho, S., Hossain, M.S.B., Halpenny, T., Archniegas, C., Dranetz, J., Hadley, D., Guo, Z., Choi, H., 2025. Ultra-mocap: A multimodal imu and semg dataset for upper body joint kinematics analysis. *Authorea Preprints*.
- G B, K., R N, P., Goel, S., 2023. Accuracy improved muscle onset and termination detection in emg signal processing using stkeo, in: 2023 16th International Conference on Sensing Technology (ICST), pp. 1–6. doi:10.1109/ICST59744.2023.10460860.
- Gan, Z., Bai, Y., Wu, P., Xiong, B., Zeng, N., Zou, F., Li, J., Guo, F., He, D., 2025. Sgrn: Semg-based gesture recognition network with multi-dimensional feature extraction and multi-branch information fusion. *Expert Systems with Applications* 259, 125302.
- Heckman, C., Enoka, R.M., 2012. Motor unit. *Comprehensive physiology*, 2629–2682.
- Henneman, E., Somjen, G., Carpenter, D.O., 1965. Functional significance of cell size in spinal motoneurons. *Journal of neurophysiology* 28, 560–580.
- Hsu, W.N., Bolte, B., Tsai, Y.H.H., Lakhotia, K., Salakhutdinov, R., Mohamed, A., 2021. Hubert: Self-supervised speech representation learning by masked prediction of hidden units. *IEEE/ACM transactions on audio, speech, and language processing* 29, 3451–3460.
- Huang, X., Xiao, J., Chang, Q., Fang, B., 2025. An onset detection method for slowly activated muscle based on marginal spectrum entropy. *Sensors* 25. URL: <https://www.mdpi.com/1424-8220/25/10/2963>.
- Jenkins, G., Tortora, G.J., 2016. *Anatomy and physiology*. John Wiley & Sons.
- Kang, K., Rhee, K., Shin, H.C., 2020. Event detection of muscle activation using an electromyogram. *Applied Sciences* 10. URL: <https://www.mdpi.com/2076-3417/10/16/5593>.
- Karnam, N.K., Turlapaty, A.C., Dubey, S.R., Gokaraju, B., 2023. Emaha-db1: A new upper limb semg dataset for classification of activities of daily living. *IEEE Transactions on Instrumentation and Measurement* 72, 1–11. doi:10.1109/TIM.2023.3279873.
- Khoshdel, V., Akbarzadeh, A., Naghavi, N., Sharifnezhad, A., Souzanchi-Kashani, M., 2018. semg-based impedance control for lower-limb rehabilitation robot. *Intelligent Service Robotics* 11, 97–108.
- Kim, M., Kim, K., Chung, W.K., 2018. Simple and fast compensation of semg interface rotation for robust hand motion recognition. *IEEE Transactions on Neural Systems and Rehabilitation Engineering* 26, 2397–2406.

- Kotov-Smolenskiy, A., Khizhnikova, A., Klochkov, A., Suponeva, N., Piradov, M., 2021. Surface emg: applicability in the motion analysis and opportunities for practical rehabilitation. *Human Physiology* 47, 237–247.
- Lacerda, L.T., Costa, C.G., Lima, F.V., Martins-Costa, H.C., Diniz, R.C., Andrade, A.G., Peixoto, G.H., Bembem, M.G., Chagas, M.H., 2019. Longer concentric action increases muscle activation and neuromuscular fatigue responses in protocols equalized by repetition duration. *The Journal of Strength & Conditioning Research* 33, 1629–1639.
- Li, M., Wei, Z., Zhang, Z.Q., Yang, B., Xie, S.Q., 2026. A conditional gan-based framework for sparse semg data augmentation with muscle synergy prior constraints. *IEEE Journal of Biomedical and Health Informatics*, 1–14doi:10.1109/JBHI.2026.3656514.
- Lim, J., Lu, L., Goonewardena, K., Liu, J.Z., Tan, Y., 2024. Assessment of self-report, palpation, and surface electromyography dataset during isometric muscle contraction. *Scientific Data* 11, 208.
- Lin, R., Wang, F., Kawata, S., Zhao, J., She, J., Chugo, D., 2024. Reducing the influence of individual variability in semg-based fatigue detection using transfer learning, in: 2024 IEEE Conference on Pervasive and Intelligent Computing (PICom), IEEE. pp. 142–147.
- Lin, Z., Liang, P., Zhang, X., Qin, Z., 2023. Toward robust high-density emg pattern recognition using generative adversarial network and convolutional neural network, in: 2023 11th International IEEE/EMBS Conference on Neural Engineering (NER), IEEE. pp. 1–5.
- Martens, J., Daly, D., Deschamps, K., Fernandes, R.J.P., Staes, F., 2015. Intra-individual variability of surface electromyography in front crawl swimming. *PLoS one* 10, e0144998.
- Merletti, R., Farina, D., 2016. *Surface electromyography: physiology, engineering, and applications*. John Wiley & Sons.
- Micera, S., Sabatini, A.M., Dario, P., 1998. An algorithm for detecting the onset of muscle contraction by emg signal processing. *Medical engineering & physics* 20, 211–215.
- Milner-Brown, H., Stein, R., Yemm, R., 1973. The contractile properties of human motor units during voluntary isometric contractions. *The Journal of physiology* 228, 285–306.
- Montazerin, M., Zabihi, S., Rahimian, E., Mohammadi, A., Naderkhani, F., 2022. Vit-hgr: vision transformer-based hand gesture recognition from high density surface emg signals, in: 2022 44th Annual International Conference of the IEEE Engineering in Medicine & Biology Society (EMBC), IEEE. pp. 5115–5119.
- Morantes, G., Fernández, G., Altuve, M., 2013. A threshold-based approach for muscle contraction detection from surface emg signals, in: IX International Seminar on Medical Information Processing and Analysis, SPIE. pp. 90–100.
- Moreira, L., Figueiredo, J., Fonseca, P., Vilas-Boas, J.P., Santos, C.P., 2021. Lower limb kinematic, kinetic, and emg data from young healthy humans during walking at controlled speeds. *Scientific data* 8, 103.
- Nasrallah, C., Boudaoud, S., Laforet, J., Chazard, E., Beuscart, J.B., Istrate, D., 2023. semg signal generation for data augmentation using time series transformer based conditional gan, in: 2023 Seventh International Conference on Advances in Biomedical Engineering (ICABME), pp. 137–141. doi:10.1109/ICABME59496.2023.10293077.
- Nazmi, N., Yamamoto, S.I., Rohim, M.A.S., Shair, E.F., 2024. Classification of gait phases by using svm and ann based on emg signals, in: 2024 IEEE Symposium on Industrial Electronics & Applications (ISIEA), pp. 1–6. doi:10.1109/ISIEA61920.2024.10607348.
- Oskoei, M.A., Hu, H., 2008. Support vector machine-based classification scheme for myoelectric control applied to upper limb. *IEEE Transactions on Biomedical Engineering* 55, 1956–1965. doi:10.1109/TBME.2008.919734.
- Özgül, K.T., Çelik, U., Kurdak, S.S., 2010. Determination of an optimal threshold value for muscle activity detection in emg analysis. *Journal of sports science & medicine* 9, 620.
- Phinyomark, A., Phukpattaranont, P., Limsakul, C., 2012. Feature reduction and selection for emg signal classification. *Expert systems with applications* 39, 7420–7431.
- PRASAD, V., SAI B, L.N., et al., 2024. Feature extraction and classification of different hand movements from the emg signal using linear discriminant analysis classifier. *i-manager's Journal on Electronics Engineering* 14.
- She, Q., Luo, Z., Meng, M., Xu, P., 2010. Multiple kernel learning svm-based emg pattern classification for lower limb control, in: 2010 11th International Conference on Control Automation Robotics & Vision, IEEE. pp. 2109–2113.
- Staudenmann, D., Roeleveld, K., Stegeman, D.F., Van Dieën, J.H., 2010. Methodological aspects of semg recordings for force estimation—a tutorial and review. *Journal of electromyography and kinesiology* 20, 375–387.
- Sun, J., Wang, Y., Hou, J., Li, G., Sun, B., Lu, P., 2024a. Deep learning for electromyographic lower-limb motion signal classification using residual learning. *IEEE Transactions on Neural Systems and Rehabilitation Engineering* 32, 2078–2086. doi:10.1109/TNSRE.2024.3403723.
- Sun, J., Wang, Y., Hou, J., Li, G., Sun, B., Lu, P., 2024b. Deep learning for electromyographic lower-limb motion signal classification using residual learning. *IEEE Transactions on Neural Systems and Rehabilitation Engineering* 32, 2078–2086. doi:10.1109/TNSRE.2024.3403723.
- Taborri, J., Keogh, J., Kos, A., Santuz, A., Umek, A., Urbanczyk, C., van der Kruk, E., Rossi, S., 2020. Sport biomechanics applications using inertial, force, and emg sensors: A literature overview. *Applied bionics and biomechanics* 2020, 2041549.
- Torres-Peralta, R., Losa-Reyna, J., González-Izal, M., Perez-Suarez, I., Calle-Herrero, J., Izquierdo, M., Calbet, J.A., 2014. Muscle activation during exercise in severe acute hypoxia: role of absolute and relative intensity. *High Altitude Medicine & Biology* 15, 472–482.
- Tu, P., Li, J., Wang, H., Li, Y., Xiang, W., 2023. A novel lower-limb coordination assessment scheme using multi-scale nonlinear coupling characteristics with semg. *IEEE Transactions on Instrumentation and Measurement* 72, 1–11.
- Valentin, S., Zsoldos, R.R., 2016. Surface electromyography in animal biomechanics: A systematic review. *Journal of Electromyography and Kinesiology* 28, 167–183.
- Wang, Z., Yao, J., Xu, M., Jiang, M., Su, J., 2024. Transformer-based network with temporal depthwise convolutions for semg recognition. *Pattern Recognition* 145, 109967. URL: <https://www.sciencedirect.com/science/article/pii/S0031320323006659>, doi:<https://doi.org/10.1016/j.patcog.2023.109967>.
- Wei, W., Tan, F., Zhang, H., Mao, H., Fu, M., Samuel, O.W., Li, G., 2023. Surface electromyogram, kinematic, and kinetic dataset of lower limb walking for movement intent recognition. *Scientific Data* 10, 358.
- Wei, W., Wong, Y., Du, Y., Hu, Y., Kankanhalli, M., Geng, W., 2019. A multi-stream convolutional neural network for semg-based gesture recognition in muscle-computer interface. *Pattern Recognition Letters* 119, 131–138.

- Xiao, F., 2022. Ewt-ii: a surface electromyography denoising method. *Medical & Biological Engineering & Computing* 60, 3509–3523.
- Yu, X., Xiong, S., 2019. A dynamic time warping based algorithm to evaluate kinect-enabled home-based physical rehabilitation exercises for older people. *Sensors* 19, 2882.
- Zeghidour, N., Luebs, A., Omran, A., Skoglund, J., Tagliasacchi, M., 2021. Soundstream: An end-to-end neural audio codec. *IEEE/ACM Transactions on Audio, Speech, and Language Processing* 30, 495–507.
- Zhang, H., Zhao, Y., Yao, F., Xu, L., Shang, P., Li, G., 2013. An adaptation strategy of using lda classifier for emg pattern recognition, in: 2013 35th Annual International Conference of the IEEE Engineering in Medicine and Biology Society (EMBC), pp. 4267–4270. doi:10.1109/EMBC.2013.6610488.
- Zhang, L., Li, Y., Xu, Z., Tian, Y., 2012. Noise reduction of semg by svd based on neural network, in: Proceedings of the 10th World Congress on Intelligent Control and Automation, IEEE. pp. 5035–5039.
- Zhang, X., Qu, Y., Zhang, G., Wang, Z., Chen, C., Xu, X., 2025. Review of semg for exoskeleton robots: Motion intention recognition techniques and applications. *Sensors* 25. URL: <https://www.mdpi.com/1424-8220/25/8/2448>.